# Gamma oscillations underlying the visual motion aftereffect

Alexander Tikhonov,[a,1] Barbara Händel,[a,b,1] Thomas Haarmeier,[a,b]
Werner Lutzenberger,[c] and Peter Thier[a,*]

[a]Department of Cognitive Neurology, Hertie Institute for Clinical Brain Research, Hoppe-Seyler-Straße 3, 72076 Tübingen, Germany
[b]Department of General Neurology, Hertie Institute for Clinical Brain Research, University of Tübingen, 72076 Tübingen, Germany
[c]Institute of Medical Psychology and Behavioural Neurobiology, University of Tübingen, 72076 Tübingen, Germany

After having been exposed to strong visual motion in one direction, a subsequently presented stationary visual scene seems to move in the opposite direction. This motion aftereffect (MAE) is usually ascribed to short-term functional changes in cortical areas involved in visual motion analysis akin to adaptation. Using magnetoencephalography (MEG), we show increased global field activity due to the MAE which could mostly be explained by a dipole located near the putative location of human area MT+. We further demonstrate that the induced MAE is accompanied by a significant increase in gamma-band activity (GBA) recorded from parietooccipital cortex contralateral to the visual motion stimulus. This gamma oscillation most likely reflects an increase in neuronal response coherence due to decreased inhibition of a group of neurons with similar preferred direction, namely the direction opposite to the adapted one. A second focal GBA response was picked up by the most posterior sensors ipsilateral to the side of the stimulus, reflecting the size of the MAE, whose source could not be reliably located.
© 2007 Elsevier Inc. All rights reserved.

*Keywords:* Magnetoencephalography; Gamma-band activity; Coherence

## Introduction

Since the report of high frequency oscillation in the octopus retina (Fröhlich, 1913) a lot of work has been conducted in an attempt to unravel the neuronal basis and the functional role of the so called gamma oscillations. Besides the differentiation in at least three different types, i.e., evoked (phase locked), induced (non-phase locked) and baseline gamma activity (for a review see Bertrand and Tallon-Baudry, 2000; Müller et al., 2000) several hypothesis have tried to explain its functionality. One influential idea has been the suggestion that the synchronization of regional gamma oscillations may underlie the formation of a coherent percept, based on elementary stimulus features, assumed to be represented in distinct cortical areas, thereby needed to be bound (the "binding problem", see Singer, 1999; Gray, 1999 for review).

Increasing evidence indeed suggests that neuronal gamma-band (40–100 Hz) synchronization is a fundamental process involved in several important brain functions, including visual feature binding (Eckhorn et al., 1998; Gray and Singer, 1989; Tallon-Baudry et al., 1996; Tallon-Baudry et al., 1997; Lutzenberger et al., 1995; Freunberger et al., 2007; Kaiser et al., 2004; Herrmann et al., 1999; Müller et al., 1996; Krishnan et al., 2005), bistable percept (Rodriguez et al., 1999; Lachaux et al., 2005; Keil et al., 1999; Müller et al., 2000; Basar-Eroglu et al., 1996), attentional stimulus selection (Lakatosa et al., 2004; Fries et al., 2001; Sokolov et al., 1999; Gruber et al., 1999; Tallon-Baudry et al., 2005), working memory (Tallon-Baudry et al., 1998; Lutzenberger et al., 2002) and associative learning (Miltner et al., 1999). For overview see Tallon-Baudry (2003), Basar-Eroglu et al. (1996), Engel and Singer (2001), Kaiser and Lutzenberger (2004) and Kahana (2006).

Up to now, the involvement of gamma oscillations in visual perception has, with two exceptions, been explored in humans by using stimuli in which changes of stimulus features underlie changes in perception. Only two groups used perceptually ambiguous stimuli. Besides an early study, which revealed increased gamma-band activity (GBA) selectively during the reversal of an ambiguous motion percept over the whole cortex (Basar-Eroglu et al., 1996), a later study could show that horizontal motion involving perceived movement from the left to the right visual hemifield induced synchronization between occipital sensors lying over the left and right hemisphere. This synchronization was not observed if the ambiguous motion was observed as moving vertically in only one hemifield (Rose and Büchel, 2005). However, both groups compared two different but equally valid perceptual states rather than a state characterized by the presence of a percept vs. a state in which the same percept was absent, although the visual stimulus was still available. We therefore asked if we could detect a difference in GBA for a situation in which a percept was present or absent independent of the visual input. To this end we used the motion aftereffect (MAE) which describes illusory

---

motion perception due to prolonged exposure to strong visual motion in one direction. A second important question we wanted to answer was if GBA representing perceptual states would be visible over the sites of primary visual processing or rather at a higher level.

Efforts to locate the structural and the physiological basis of the MAE as yet have relied on single-unit recordings from the visual cortex of monkeys (Petersen et al., 1985; Kohn and Movshon, 2003) and fMRI (Tootell et al., 1995; He et al., 1998; Culham et al., 1999; Taylor et al., 2000) and PET (Hautzel et al., 2001) studies of the human brain, jointly singling out area MT and neighboring cortex as the major substrate of the MAE. Additional evidence for a role of human MT+ comes from studies using repetitive transcranial magnetic stimulation (TMS) which could show that TMS of human MT+ disrupted the perception of the MAE (Théoret et al., 2002).

In an attempt to capture high frequency oscillations possibly underlying the MAE we used magnetoencephalography (MEG). We found increased GBA over parietooccipital sensors and an increased strength in dipoles located near the putative location of human area MT+ for the MAE compared to the no-MAE condition. An additional focus of GBA whose signal amplitude correlated with the size of the MAE could not be located to a specific region. Possible sources of this second focus will be discussed.

## Methods

### Subjects

Eight subjects (two females, mean age 28.0 years) in experiment 1 and 9 subjects in experiment 2 (four females, mean age 28.0 years) gave their informed and written consent to participate in the study after having the experimental protocol explained to them. All of the subjects had normal or corrected to normal vision, were right-handed and had no history of neurological disease. The experimental protocol of the study had been approved by the ethics committee of the Tübingen Medical Faculty.

### Stimuli

Stimuli were rear projected onto a large translucent screen (DLP Projector, frame rate 60 Hz, 800 × 600 pixel) positioned at a viewing distance of 92 cm in a magnetically shielded room. Viewing was binocular.

A red spot (diameter 10 min of arc), presented in the middle of the screen, served as a gaze fixation target during the whole trial. The visual motion stimuli were projected unilaterally into the right (experiment 1) and the left (experiment 2) visual hemifield, respectively, at an eccentricity of 12.5° (fixation spot to middle of the motion stimulus) on the horizontal meridian. Stimuli subtended a visual angle of 9 × 9° and consisted of 300 white dots (diameter: 15 arc min; luminance: 65 cd/m$^2$; individual lifetime: 200 ms) which were randomly plotted on a dark background. Dots that left the stimulus aperture were re-plotted in randomly chosen positions within the aperture. Each experimental trial (see Fig. 1) began with a *blank interval* (duration 0.5 s), in which only the central fixation spot was visible. This interval was followed by a *priming phase* lasting 5.0 s during which a random dot pattern (RDP) was presented (Fig. 1). Different for two conditions applied, the 300 dot elements would either move coherently downward (MAE condition) or would move in individually varying directions (*motion-balanced*) drawn from a distribution of directions spanning 360° (no-MAE condition). After a subsequent second *blank interval* (0.4 s) the *test phase* (duration: 0.5 s) started. In this test phase, again an RDP was presented in which the dots moved in individually varying directions as described for the priming phase of the no-MAE condition. When presented in isolation, this *motion-balanced* RDP lacked global motion and appeared as a flickering, globally stationary pattern. However, when preceded by
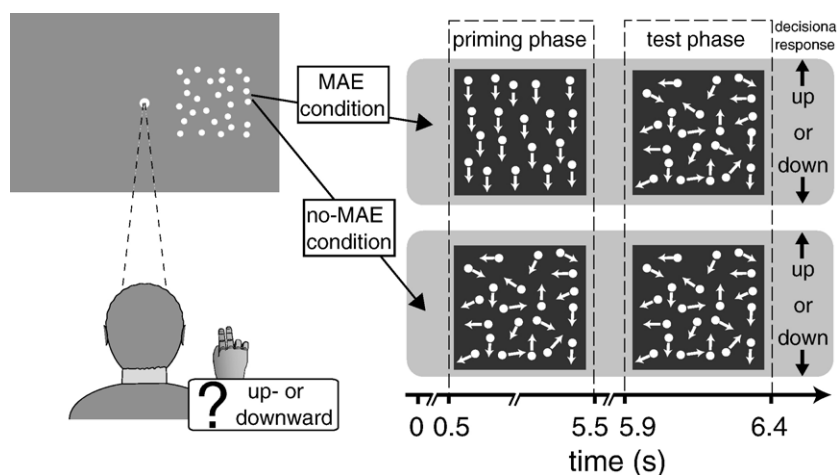


Fig. 1. Experimental paradigm. Sequence of events in an experimental trial. The random dot pattern (RDP) was presented always right of the fixation spot in experiment 1 and left of the fixation spot in experiment 2. Dashed lines indicate the time of presentation of the RDP. In the priming phase, downward moving coherent RDP was presented in the MAE condition, whereas, alternatively, a motion-balanced RDP in which dots moved in random directions was used in the no-MAE condition. In the subsequent test phase, an RDP was presented in both conditions, in which the individual dots moved in random directions. Whereas in MEG trials the net motion was balanced, in psychophysical trials (not shown here) a vertical motion component of varying size was added in order to titrate the size of the MAE. Subjects reported the perceived direction (up- or downward) of the global motion of the RDP in the test phase by lifting the middle finger (motion upward) or the index finger (motion downward) of their right hand (two-alternative choice).

a coherent RDP as in the MAE condition it seemed to move upward, i.e., in a direction opposite to that of the priming stimulus due to the motion aftereffect induced. At the end of each trial, subjects were required to indicate their perceived direction of global motion of the second RDP by lifting their index finger (perception of downward motion) or middle finger (perception of upward motion) of their right hand (experiment 1 and 2). Trials with coherent and incoherent visual motion during the priming phase (MAE versus no-MAE condition) were presented in two subsequent blocks. The sequence of these two blocks was pseudo-randomized across subjects.

Trials as described so far were shown in 75% of all presentations and were termed *MEG trials* because only they contributed to the MEG records. In the remaining 25% of trials, called *psychophysical trials*, there was a change in the stimulus concerning its test phase. In the MEG trials the test phase lacked coherent motion as described above. However, in the *psychophysical* trials the motion-balanced RDP underlying the test phase stimuli was biased by introducing a constant amount of vertical motion added vectorially to all dot elements. The movement of each individual dot was given by summing the vertical bias vector, which was the same for all dots, and the individual dot velocity vector underlying the unbiased motion-balanced RDP. If the size of the biased motion vector corresponded to the size of the oppositely directed MAE, the physical motion and the illusory motion annihilated each other, rendering the biased *motion-balanced RDP* perceptually stationary. In order to determine the size of the vertical (downward) motion bias needed to render the stimulus stationary (velocity of subjective stationarity), its size was varied from psychophysical trial to psychophysical trial by a PEST staircase procedure (Taylor and Creelman, 1967; Lieberman and Pentland, 1982). The velocity of subjective stationarity at which subjects will guess the direction of global motion as indicated by equal numbers of upward and downward decisions was determined by means of a probit analysis (McKee et al., 1985) with subsequent chi-square goodness-of-fit tests performed on the responses obtained for psychophysical trials. The bias motion vector at the velocity of subjective stationarity is equal in size but opposite in direction to the MAE and may therefore serve as an operational measure of the MAE. Given the fact that the psychophysical trials were presented randomly interleaved with the MEG trials, we assumed that this measure of the MAE based on psychophysical trials was representative of the MAE in MEG trials as well. We felt that titrating the size of the MAE, prompted by the presentation of the incoherently moving dots quantitatively in this way, was preferable to asking subjects simply whether an MAE is present or absent when viewing a stationary test pattern and to measuring the duration of the percept as has been custom in previous studies (e.g. Culham et al., 1999; Taylor et al., 2000; Hautzel et al., 2001).

A full block of trials comprised 120 MEG trials, independent of the actual number of psychophysical trials, of either the MAE or no-MAE condition.

### Recording of eye movements

Subjects were instructed to fixate the central fixation spot as accurately as possible while avoiding head movements. Head movements were further reduced by employing a bite bar, attached to the MEG chair. During all experiments, eye movements were monitored using a 50 Hz home made video based eyetracker. The means of eye velocity and the frequency of saccades during background presentation were calculated offline for each individual subject for the different classes of trials. Only trials accompanied by fixation within a 3° fixation window were accepted for further analysis.

### MEG recordings

MEG was recorded using a whole-head system (CTF Inc. Vancouver, Canada) comprising 151 first-order magnetic gradiometers. The signals were sampled at a rate of 625 Hz with a 200 Hz anti-aliasing filter. The MEG records were resampled offline to 312.5 Hz. One of the sensors located over the left frontal cortex (LF13) had to be excluded from later analysis because of a technical dysfunction during recordings (first experiment). In a second experiment two sensors (LT15, RP11) had to be excluded. Fixation point onset at the beginning of each trial started the sampling. The total sampling epoch per trial was 6400 ms and lasted up to the end of the test phase. Subjects' head position was monitored using a set of three magnetic head localization coils attached to the nasion and two preauricular reference points. Head position measurements were conducted at the beginning and at the end of each experimental block (120 MEG trials) in order to verify the stability of head orientation.

### Analysis of neuromagnetic activity

To investigate the spectral, temporal and spatial aspects of the MEG activity associated with the percept of MAE, the following approaches were used.

### Analysis of the global field power

In a first attempt to search for MEG activity reflecting the MAE, we analyzed the global field power (GFP). In order to obtain the GFP, the MEG recordings were first of all baseline corrected with respect to an interval ranging from −100 to 0 ms before test phase onset which corresponds to the 100 ms blank period between priming phase and test phase. The recordings were then digitally low-pass filtered at 40 Hz and averaged over trials for the two conditions (i.e., MAE and no-MAE) and each subject. Based on these averages, the global field power was calculated for the MAE and no-MAE condition as the root of the mean squared magnetic fields (RMS) of all sensors for each sample and for each subject.

### Dipole analysis

An equivalent current dipole (ECD) model was calculated using the averaged magnetic field independent of the condition for each subject separately over the first 250 ms of the test phase of the trial. A representative individual spherical head model was used and the corresponding ECDs were determined by a least-square minimization procedure based on running standard BESA and CTF software. For each subject the individual dipole positions were mapped into the Talairach stereotactic standard space. In a second step neuromagnetic activity averaged separately over the two conditions (MAE and no-MAE) was modeled using the previously obtained dipole locations. Dipoles were determined as previously described but in order to elucidate the temporal dynamic, dipole strength was extracted for the whole time period of the test phase. ECD moments obtained for the two conditions were then subtracted and time periods in which the difference exceeded the baseline noise level (3 times STD)

calculated at the 50 ms pre-stimulus interval were identified. In addition a regression was calculated between the difference of the mean dipole moment of the first 250 ms of the test phase for the MAE and the no-MAE condition and the difference of the percept in the two conditions. This regression was carried out separately for the two dipoles considered and showed no significant effect ($p > 0.05$).

*Spectral analysis*

Spectral analysis was carried out in order to identify high frequency oscillations (40–100 Hz) connected to the MAE.

To this end, the MEG signals recorded during the test phase were analyzed on a single trial basis. Selecting this time window of 500 ms resulted in 156 samples (sampling rate 312.5 Hz), which were zero-padded to obtain 256 points. To these data points a Welch window was applied and a Fast Fourier transformation (frequency resolution: 1.221 Hz) was conducted. The square roots of the obtained power values were then averaged across trials for each frequency bin, sensor, experimental condition and subject. Differences in power between the MAE and no-MAE condition were assessed for each sensor and each frequency bin (within a range from 40 Hz to 100 Hz) by applying a *t*-test. In order to correct for multiple comparison, a statistical sensor analysis (SSA) was performed, as described in detail further below.

We not only wanted to analyze the group differences between conditions but also if the percept of the MAE would be reflected in the MEG signal. We therefore searched for significant linear correlations between the perceptual differences between the MAE and the no-MAE condition of the individuals and the corresponding individual differences in spectral power for each sensor and for each frequency bin. The correlation coefficients obtained from linear regressions were transformed to *t*-values and their significance was tested again by the statistical sensor analysis conducted as follows.

*Statistical sensor analysis*

Statistical sensor analysis (SSA) was based on randomization tests (Blair and Karniski, 1993; Noreen, 1989; Kaiser et al., 2006) and included corrections both for multiple comparisons and for possible correlations between data from neighboring frequency bins and sensors. In general, permutation analysis estimates the significance of actual test values by applying the identical tests to simulated data, obtained by permutation of the actual observations. The significance criterion is estimated on the basis of the permuted data in such a manner that the critical test value is the one for which 5% of the test values are greater. If the test value of the original data lies above this critical test value the statistical test is considered significant. One concern, however, was that differences between conditions restricted to one sensor or one frequency bin only are taken as significant even though such events are extremely unlikely, especially as we take quite small frequency bins into account (1.2 Hz). To exclude this possibility, we additionally further demanded that always two neighboring frequency bins or sensors had to show a significant effect. To this end we used a slightly altered method as has been described previously by Lutzenberger et al. in 2002. To demand two neighboring events to be significant at the same time is a quite common approach (e.g. Fell et al., 2001; Trautner et al., 2006).

In a first step, test-specific statistics (i.e., *t*-test or linear correlation, respectively) were evaluated for each sensor (total = 150 sensors) and each frequency bin (width 1.221 Hz, band of 40–

100 Hz, total = 48) resulting in a first distribution of test values. To ensure that tests for two neighboring frequency bins and sensors were significant, a new distribution of minimal test values was determined for all pairs of neighboring frequency bins and sensors by taking only the *smaller* one of the neighbors into account. Now P0.05 was determined as the *p*-value corresponding to the test value from the new distribution for which 5% of the observed *minimal* test values were greater. In the case of highly correlated data, P0.05 would be ≤0.05, whereas for highly independent data, P0.05 would be >0.05 (Kaiser et al., 2000; Lutzenberger et al., 2002).

In a second step, the corresponding distribution of *maximal* test values was calculated for the *permuted* data sets, taking only the *larger* test value of all pairs of neighboring frequency bins and sensors into account. Based on this distribution the critical test value tcrit was defined as the test value where P0.05 × number of permutations of the obtained maximal test values were greater. The obtained critical *t*-value tcrit was then applied as criterion of significance to the observed original data (Lutzenberger et al., 2002).

Permutations were conducted as follows. For the group statistics (*t*-test), data from all sensors and frequency bins were exchanged between the two experimental conditions (MAE and no-MAE conditions) for one or several subjects chosen by chance (number of permutations = $2^n$; with $n = 8$ for experiment 1; $n = 9$ for experiment 2). For the correlation analysis data from all sensors and all frequency bins were permuted across individuals resulting in a new pairing between perceptual data (difference in MAE between conditions) and brain activity (difference in spectral amplitude between conditions). The number of permutations made in that way was 8000; each of those was randomly selected out of $n!$ ($n$ = number of subjects) its possible number.

*Time course analysis*

Having identified those MEG signals showing a significant effect in the group and correlation analysis we tried to capture the time course of these. To this end, the signal at the time of interest (test phase) was padded to 312 samples by mirroring the first 16 samples of the signal to the temporal interval prior to the signal and the final 16 samples of the signal were mirrored to the temporal interval subsequent to the signal. The mirrored portions now were multiplied with cosine windows, centered either on the first sample of the signal (for the first padded portion) or centered on the last sample (for the final padded portion). The so treated signal was now bandpass filtered using a Gaussian curve-shaped Gabor filter (width: 2.5 Hz) centered on the frequency range for which the preceding analysis had yielded significant effects. The filtered data were now amplitude-demodulated by means of a Hilbert transformation (Clochon et al., 1996). The resulting representation of the time course of the amplitude in the filtered frequency band was used to investigate the time course of the previously found effects, i.e., group differences between conditions and the correlation of the spectral amplitude with the MAE of the individual subject, respectively. For the first mentioned, the amplitude values, averaged across trials in each subject, were compared between conditions for every point in time using a running *t*-test. For the second effect mentioned, a correlation between the difference in perceived MAE and the difference in spectral amplitude between the two conditions was evaluated over the subjects for each time point by a running linear regression. SSA was used as described above to test for significance taking the correlation between consecutive time points into account.

## Results

For the eight subjects participating in experiment 1, the mean MAE in the MAE condition amounted to 2.9°/s (Fig. 2A), i.e., corresponding to the perception of upward motion while watching the motion balanced RDP. Surprisingly, the mean measured MAE in the absence of a priming stimulus deviated significantly from zero as well (1.6°/s). A psychophysically measured MAE in the absence of induced motion is likely to reflect a response bias for upward motion. Hence, it is the significant increase in the size of the mean MAE by 1.3°/s (one-sided paired $t$-test, $p < 0.0001$) obtained for the MAE condition compared to the no-MAE condition that reflects the true size of the MAE. Importantly, this perceptual difference was not paralleled by any differences in the quality of fixation as indicated by the fact that the residual eye velocities were the same during the presentation of the test stimulus in the two conditions (running paired $t$-tests, for all samples of the test phase; $p > 0.05$). Moreover, we did not find a significant correlation between the individual differences in the size of the MAE in the two conditions and the individual quality of fixation as assessed by calculating the difference in mean retinal image velocity between conditions ($p > 0.05$).

In order to determine those MEG components which differed significantly between the two conditions (MAE versus no-MAE) during the presentation of the MEG stimulus we first looked at the global field power (GFP). The upper 3 panels of Fig. 3A show the group averages of evoked neuromagnetic responses (8 subjects, 150 sensors overlaid) as a function of time for the two conditions and their difference. Time during the presentation of RDP in the test phase of the trial (500 ms, gray area) is shown as well as 50 ms prior to its onset. The lower panel depicts the mean global field power signals, i.e., the root mean squared neuromagnetic responses across all channels, averaged over all subjects for the MAE (black) and the no-MAE condition (gray). The first time period in which the difference between the two conditions surpassed the noise level by at least 3 STD is marked by broken lines (140–200 ms after stimulus onset). During this time the global field power was increased for the MAE condition. In order to localize this effect, we fitted ECDs to the magnetic field as described in the Methods section and which explained for all subjects on average 66% (±11.9%) of the overall

variance. Dipole locations modeling the magnetic field across the period of interest (first 250 ms of the RDP presentation) as calculated for both conditions are shown in Fig. 3B plotted onto a normalized brain (L: left; R: right; A: anterior; P: posterior). Open circles show the dipole positions, one lying at the occipital pole presumably in area V1 (upper panel, mean Talairach coordinates: $x = -4.07 \pm 10.38$; $y = -75.16 \pm 12.86$; $z = 6.13 \pm 17.03$), the second one lying in the lateral hemisphere contralateral to the side of visual stimulation (mean Talairach coordinates: $x = -31.74 \pm 10.98$; $y = -63.08 \pm 13.97$; $z = 24.88 \pm 16.59$), in a region most probably comprising area MT+. The lower part of Fig. 3B plots the group mean dipole moment as function of time for the two dipoles considered, separately for the two perceptual conditions. The upper lineplot (1) depicts the moments of the occipital dipole with the gray line representing trials of the no-MAE condition and black lines of the MAE condition. One can see that there is no significant difference (as defined by exceeding 3 STD of the difference measured during the 50 ms pre-stimulus time period) for the occipital dipole between MAE and no-MAE condition. However, the parietooccipital dipole depicted in the lower lineplot (2) of Fig. 3B (with identical convention) shows a significant difference for the time period between 144 and 166 ms demarcated by the two black dotted lines. Within this period of time, the dipole moment is larger for the MAE condition than for the no-MAE condition.

Using statistical sensor analysis (SSA; see Methods), we tried to determine those MEG sensors which picked up gamma-band activity (GBA) differing significantly for the group of subjects between the two conditions (MAE versus no-MAE) during the presentation of the MEG stimulus. SSA revealed an increase in GBA in the MAE condition relative to the no-MAE condition for sensors lying above left lateral parietal cortex (LLPC), i.e., contralateral to the side of the visual field stimulated. As can be drawn from Fig. 4A, which depicts the $p$-values of this group difference for all sensors, this effect reached the level of statistical significance ($p < 0.05$ after correction for multiple comparison) in one sensor located immediately adjacent to the intraparietal sulcus (sensor LP23). This increase in GBA activation was confined to a narrow frequency band of 70–71 Hz (Fig. 4B). In a second step, we correlated individual differences in the size of the MAE between the two conditions with the individual differences in spectral power
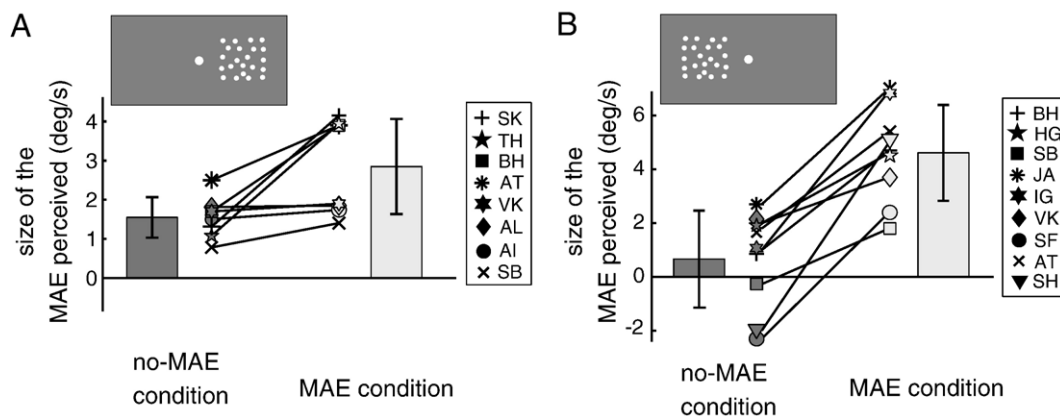


Fig. 2. Perceptual data. (A) Size of the MAE perceived in the MEG trials of the first experiment, in which the RDP was presented right of the fixation spot. The different symbols indicate individual subjects; the bars give means and standard deviations. Results are shown for the no-MAE condition (defined by the priming stimulus lacking consistent downward motion) and the MAE condition (with the priming stimulus moving coherently in downward direction). Positive velocities correspond to an upward direction of the MAE perceived. (B) Size of the MAE in the second experiment, in which the RDP was presented left of the fixation spot, same conventions as in panel A.
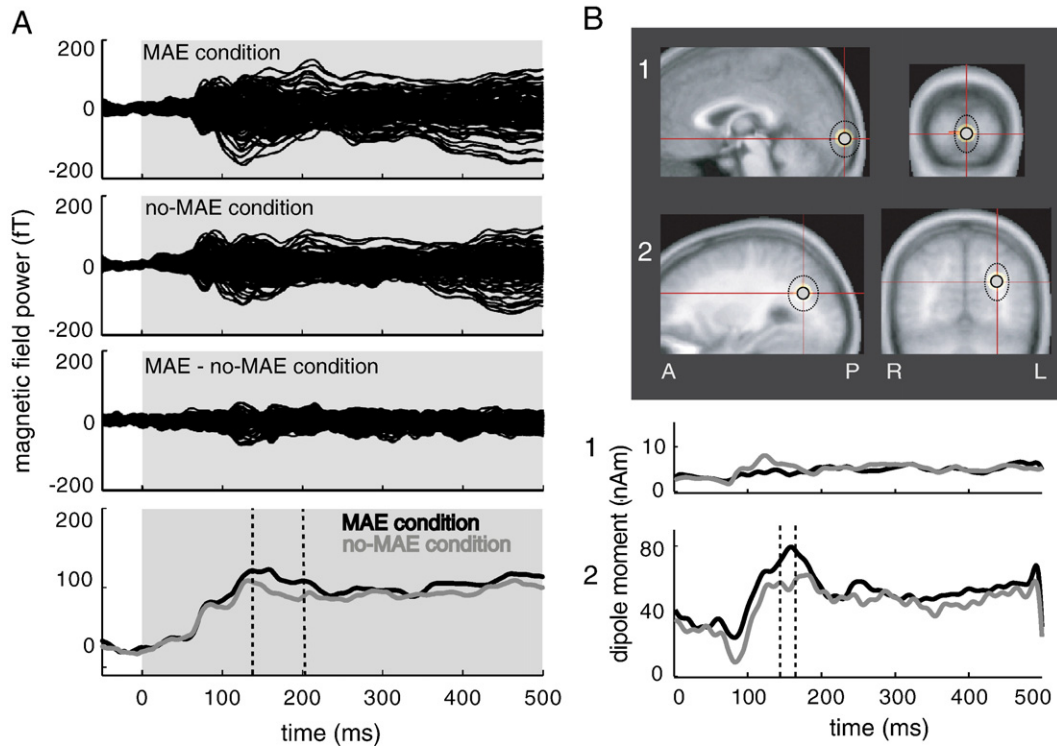
Fig. 3. Neuromagnetic responses obtained under the MAE and no-MAE condition; group data (experiment 1). (A) Upper three panels: group averages of evoked neuromagnetic responses (8 subjects, 150 sensors overlain) shown as a function of time for two conditions and their difference; MAE test phase (500 ms) is marked in gray. The fourth panel shows the mean global field power signals, i.e., the root mean squared neuromagnetic responses across all channels, averaged over all subjects for the MAE (black) and no-MAE condition (gray). The time period in which the difference between the two conditions surpassed the noise level measured during the 50 ms pre-stimulus period by at least 3 STD is marked by broken lines (140–200 ms after stimulus onset). (B) Dipole locations (open circles) modeling the magnetic field across the period of interest (first 250 ms of the RDP presentation) calculated from the data averaged over the two conditions for each subject separately (L: left; R: right; A: anterior; P: posterior). The broken circles mark the STD of the localization between subjects. The upper lineplot depicts dipole moments over time for dipole 1 (upper picture) averaged over subjects. Gray lines depict dipole moments over time obtained from trials of the no-MAE condition and black lines from the MAE condition. Dipole 2, depicted in the lower lineplot (with identical convention), shows for the time period between 144 and 166 ms a difference between conditions which surpassed the noise level measured during the 50 ms pre-stimulus period by at least 3 STD as indicated with two black dotted lines.

for each sensor and each frequency in the range of 40 to 100 Hz. As shown in Fig. 4C, the sensors that showed a linear correlation between the individual amount of change in motion perception and the individual difference in spectral power were clustered over the most inferior and posterior parts of the brain located ipsilateral to the visual field stimulated. Again, this main effect was confined to a narrow band of GBA (93–94 Hz; Fig. 4D) and survived correction for multiple comparisons in one of the sensors (sensor R041). For this sensor the linear correlation between the change in motion perception and change in spectral power was rather striking as reflected by a correlation coefficient $r$ of $-0.965$ (Fig. 4F).

The possible concern that amplitude differences were caused by individual differences in head size, location or any kind of head or neck movements can be dispelled by the fact that such changes must be expected in a quite broad frequency band. However, the effect described above as well as those that will be described below is restricted to a very narrow frequency band (see again Figs. 4B and D).

Next, in order to assess the time course of MAE associated neuromagnetic activity in the parietal sensors, we calculated the probability of finding higher GBA in the MAE condition as compared to the no-MAE condition in the frequency range of $70 \pm 2.5$ Hz for all time bins of 3.2 ms duration during the presentation of the MEG

stimulus. The analysis was confined to the sensor above the LLPC and the frequency range that had demonstrated significantly higher GBA for the MAE (marked in Fig. 4A), when the test phase as a whole had been considered. By the same token, in order to describe the time course of the percept-related neuromagnetic activity seen by the right posterior inferior sensor, we calculated the probability of the correlation between the percept and the spectral power for all time bins of 3.2 ms during the presentation of the MEG stimulus. The analysis was confined to the frequency range of (93–94, which had yielded a significant correlation between percept and oscillatory activity as calculated for the overall test phase. Fig. 4E compares the probabilities of the statistical measures for the LLPC and the right posterior sensor as a function of time. Both LLPC and right posterior sensor related $p$-values reached their respective maxima around 230 ms after the onset of the MEG stimulus. Actually, the correlation for the right posterior sensor (Fig. 4E) started to become significant even before the onset of the test stimulus (80 ms before stimulus onset, $p < 0.05$ corrected for multiple comparisons).

The validity of the findings obtained in this first experiment was tested by running a second experiment, based on nine subjects. In this second experiment all visual stimuli were flipped to the opposite side of the visual field without changing any other feature of the first experiment. In this second experiment, the mean difference of the
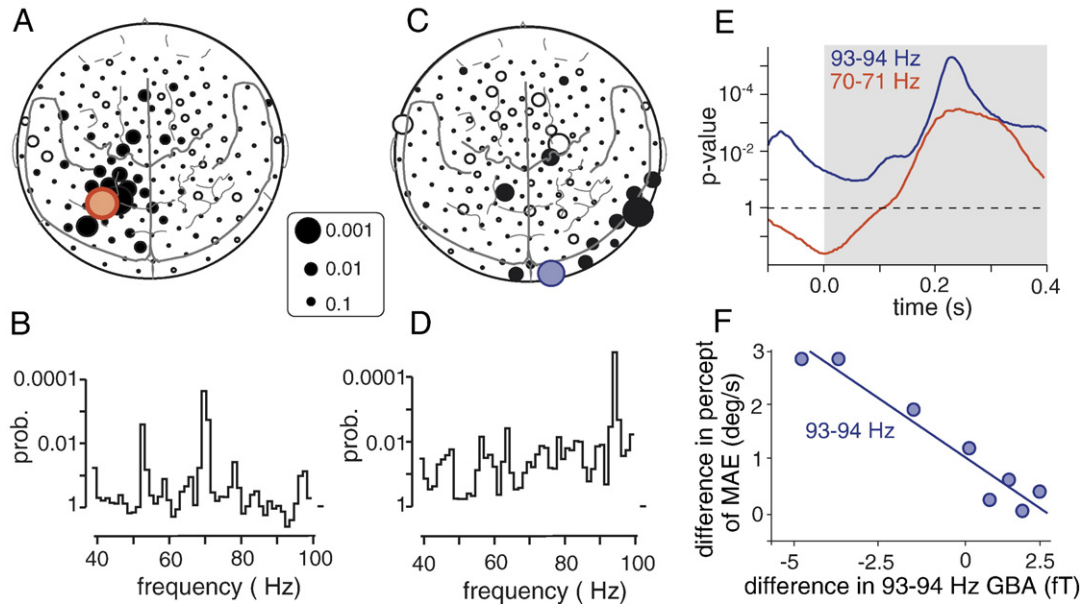
Fig. 4. MEG correlates of the MAE (experiment 1). (A) Probabilities of spectral amplitude differences in GBA 70–71 Hz) observed for the group of subjects between the MAE condition and the no-MAE condition during observation of the motion noise stimulus. The size of the sensors plotted over a flattened map of the schematic brain depicts the level of statistical significance (uncorrected), the larger the sensors the smaller the *p*-value. Filled circles mark those sensors which showed an increase in amplitude in the MAE condition compared to the no-MAE condition, open circles mark sensors with opposite dependencies. The red colored circle marks a parietal sensor (LP23) which shows a significant increase in GBA in the MAE condition ($p < 0.05$, corrected for multiple comparison). (B) Frequency distribution of the *p*-values depicting the level of statistical significance of the difference of MEG activity between the MAE and no-MAE condition recorded from sensor LP23 (marked in red color in panel A). (C) Probabilities of the correlation between the MAE and GBA mapped across all sensors of the MEG sensor array (same conventions as in panel A). Filled circles mark those sensors which show a negative correlation between the individual change in spectral GBA amplitude (93–94 Hz) and the individual change in MAE. The blue circle marks a sensor (RO41) with a significant correlation ($p < 0.05$, corrected for multiple comparison). (D) Frequency distribution of the *p*-values depicting the level of statistical significance of the correlation between GBA recorded from sensor RO41 (marked in blue color in panel B) and the MAE. (E) Time courses of GBA effects for the sensors that showed significant effects. The curves depict the results of the statistical analysis, i.e., *p*-values for time points between 100 ms before and 400 ms after test phase onset. The curves are displayed in the same colors as the corresponding sensors. *p*-values below the dashed line correspond to *t*-values and regression coefficients, respectively, favoring the alternative hypothesis. (F) The individual difference in the size of the GBA in the range of 93–94 Hz recorded from sensor RO41 for the MAE condition as compared to the non-MAE condition shows a significant correlation with the individual difference in the size of the MAE for the two conditions (8 subjects). The negative regression indicates that lesser activity corresponded to a higher MAE.

MAE between the two conditions amounted to 3.8°/s (Fig. 2B). The overall pattern of neuromagnetic responses obtained in this second experiment was similar to the one obtained in experiment 1. The main difference was that all responses changed sides.

As in experiment 1, the GFP showed a first significant increase (3 STD above noise level, marked with broken lines) in activity elicited by the MAE compared to the no-MAE condition, however, shorter in duration and at a slightly later latency (196–212 ms) as in experiment 1 (see Fig. 5A, lower panel). The upper 3 panels of Fig. 5A show the group averages of evoked neuromagnetic responses (9 subjects, 149 sensors overlaid) as a function of time for two conditions and their difference. ECDs were fitted to the magnetic field as described in the Methods section (5 subjects with a mean explained variance of 59±13.5%) and dipole locations (open circles) are shown in Fig. 5B plotted onto a normalized brain (L: left; R: right; A: anterior; P: posterior). As in experiment 1, we found one dipole lying at the occipital pole, presumably in area V1 (upper panel, mean Talairach coordinates: $x = -1.3 \pm 21.45$; $y = -95.49 \pm 20.35$; $z = -2.95 \pm 17.08$) and a second dipole, contralateral to the visually stimulated side, more lateral (mean Talairach coordinates: $x = -33.93 \pm 9.53$; $y = -59.04 \pm 15.45$; $z = 15.8 \pm 16.35$) close to the putative location of area MT+. The group mean dipole moments are plotted as functions of time separately for the two conditions (MAE=black and no-MAE=gray) in Fig. 5B (2 lowest

panels). The upper lineplot (1) depicts dipole moments for the occipital dipole. It exhibits no significant difference between conditions (as defined by exceeding 3 STD of the difference measured during the 50 ms pre-stimulus time period). However, the moment of the second, temporooccipital dipole, depicted in the lower lineplot of Fig. 5B, showed a significantly increased strength for the MAE condition for a short time period between 200 and 212 ms (demarcated by broken lines). However, these results are based only on those subjects whose magnetic fields could be fitted adequately with a two-dipole model (five out of nine), for four subjects no model could be fitted due to too large noise in the data.

Results of experiment 2 were also in good agreement with those obtained from experiment 1 regarding the GBA responses, which similar to the dipole patterns described before were characterized by a change in side. The significant increase in GBA activity on the group level for the MAE condition was now confined to the right lateral parietal cortex ($p < 0.05$ corrected, Fig. 6A) in a similar frequency range (Fig. 6B, 75–76 Hz). A significant correlation ($r = -0.880$, $p < 0.05$ corrected, frequency band 95–96 Hz) with the size of the MAE was now found for a sensor lying above the left hemisphere (Fig. 6C). Although these two effects were not observed for clusters of sensors such as in experiment 1, the location of sensors showing the statistically significant effects was almost identical for the two experiments. Specifically, the aforementioned
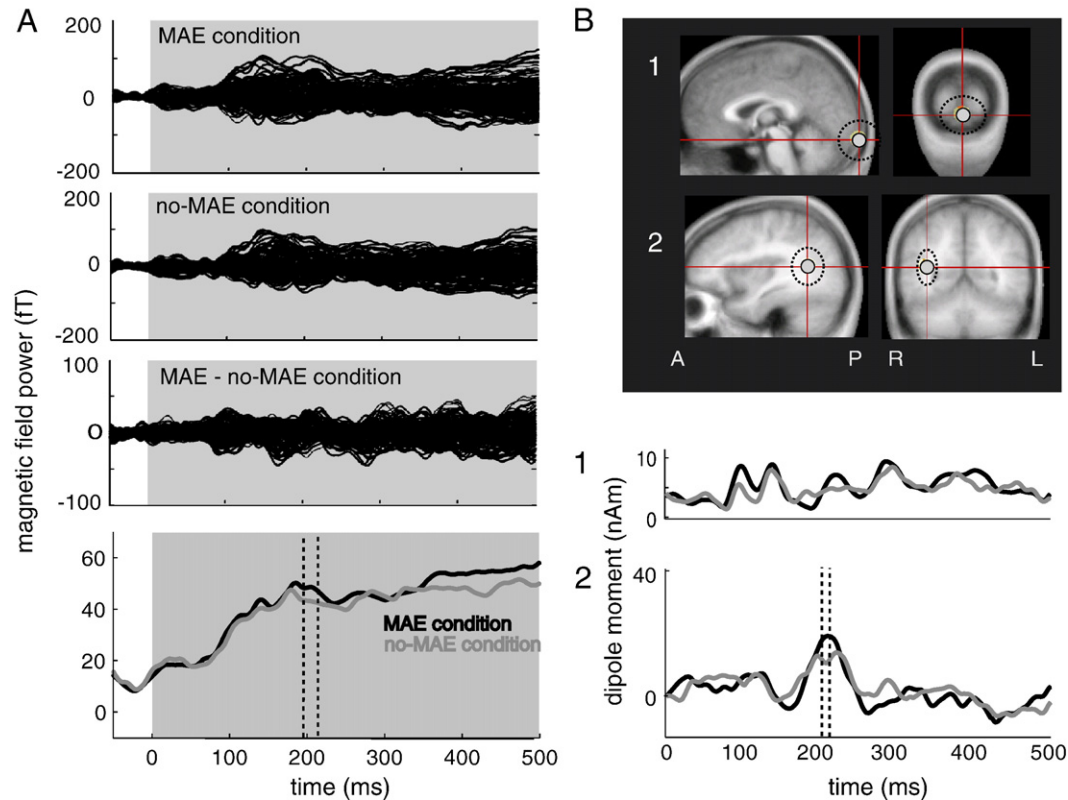
Fig. 5. Neuromagnetic responses obtained under the MAE and no-MAE condition; group data (experiment 2). (A) Upper three panels: group averages of evoked neuromagnetic responses (9 subjects, 149 sensors overlain) shown as a function of time for two conditions and their difference; MAE test phase (500 ms) is marked in gray. The fourth panel shows the mean global field power signals, i.e., the root mean squared neuromagnetic responses across all channels, averaged over all subjects for the MAE (black) and no-MAE condition (gray). The time period in which the difference between the two conditions surpassed the noise level measured during the 50 ms pre-stimulus period by at least 3 STD is marked with broken lines (196–212 ms after stimulus onset). (B) Dipole locations (open circles) modeling the magnetic field across the period of interest (first 250 ms of the RDP presentation) calculated from the data averaged over the two conditions for each subject separately (L: left; R: right; A: anterior; P: posterior). The broken circles mark the STD of the localization between the 5 subjects used for the dipole analysis. The upper lineplot depicts dipole moments over time for dipole 1 (upper picture) averaged over subjects. Gray lines depict dipole moments over time obtained from trials of the no-MAE condition and black lines from the MAE condition. Dipole 2, depicted in the lower lineplot (with identical convention), shows for the time period between 200 and 212 ms a difference between conditions which surpassed the noise level measured during the 50 ms pre-stimulus period by at least 3 STD as indicated with two black dotted lines.

increase in GBA during viewing of the MAE was associated with the right-sided sensor RP33, mirroring the left-sided LP33 – the caudal neighbor of the left LP23 – where the GBA increase had been revealed in experiment 1. The significant correlation of the GBA with the perceptual MAE, as depicted in Fig. 6F, was observed for the left posterior sensor (LT44) located a bit more rostral with respect to its contralateral analogue (RO41) that had shown a significant correlation with the MAE in experiment 1. Also, the frequency range of this effect was very similar (Fig. 6D, 95–96 Hz) compared to experiment 1. Again, we analyzed the time course of the MAE-associated effects by calculating the probability of the MAE associated difference in GBA for the parietal sensor and the probability of the correlation between the perceptual MAE and the spectral power for the ipsilateral sensor. As shown in Fig. 6E, the probability of the statistical measures for both sensors reached their maximum around 200 ms after the onset of the MEG stimulus, without, however, deviating from baseline before stimulus onset.

We did not find a significant correlation between the individual differences in spectral power of the GBA picked up by the posterior inferior sensor (experiment 1: RO41, experiment 2: LT44) and the quality of fixation as assessed by the difference in mean

retinal image velocity in the two conditions, neither for experiment 1 nor for experiment 2.

Finally, we add that we tried to delineate the underlying sources of the two MAE related gamma-band responses by means of synthetic aperture magnetometry (SAM; Robinson and Vrba, 1999). Comparing the GBA elicited by the two conditions for all subjects by considering only the relevant frequency band and all sensors during 200–400 ms after test phase onset we failed to produce a consistent localization. This, however, may not be surprising in view of the tininess of the signals at stake.

## Discussion

We used magnetoencephalography (MEG) in order to track down the neuronal circuits underlying the generation of the motion aftereffect (MAE), the illusion of visual motion associated with a stationary scene, induced by prolonged exposure to a preceding motion stimulus (Purkinje, 1825; Wohlgemuth, 1911). We observed an electrophysiological signature of the MAE in the form of increased global field power. The magnetic field distribution associated with the paradigm could be explained reasonably well by assuming two equivalent current dipole sources, a midline
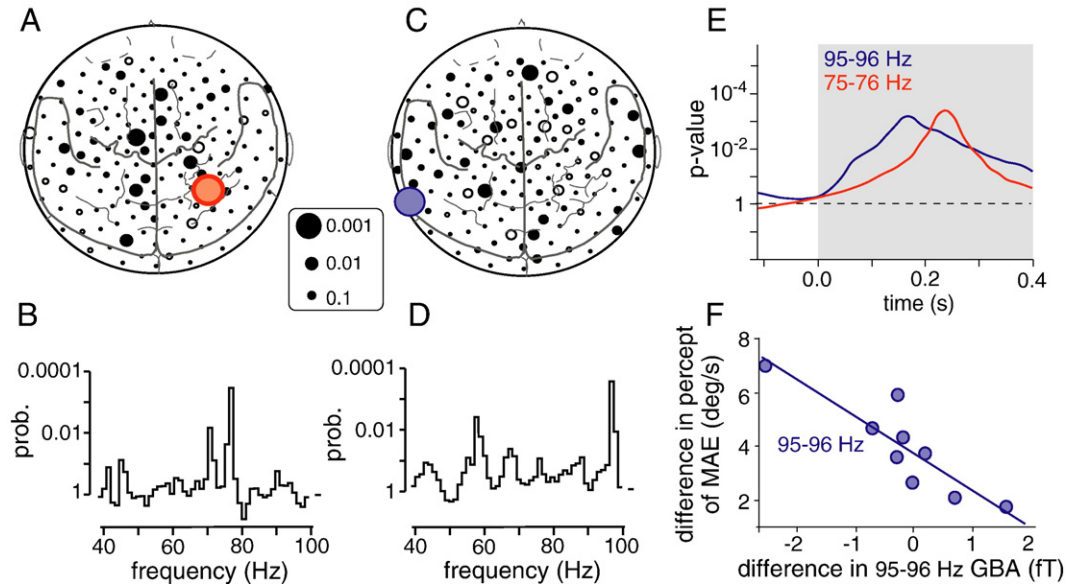
Fig. 6. MEG correlates of the MAE (experiment 2; same conventions as in Fig. 3). (A) Probabilities of spectral amplitude differences in GBA (75–76 Hz) observed for the group of subjects between the MAE condition and the no-MAE condition during observation of the motion noise stimulus. The red colored circle marks a parietal sensor (RP33) which shows a significant increase in GBA in the MAE condition ($p<0.05$, corrected for multiple comparison). (B) Frequency distribution of the $p$-values depicting the level of statistical significance of the difference of MEG activity between the MAE and no-MAE condition recorded from sensor RP33 (marked in red color in panel A). (C) Probabilities of the correlation between the MAE and GBA mapped across all sensors of the MEG sensor array. Filled circles mark those sensors which show a negative correlation between the individual change in spectral GBA amplitude (95–96 Hz) and the individual change in MAE. The blue circle marks a sensor (LT44) with a significant correlation ($p<0.05$, corrected for multiple comparison). (D) Frequency distribution of the $p$-values depicting the level of statistical significance of the correlation between GBA recorded from sensor LT44 (marked in blue color in panel B) and the MAE. (E) Time courses of GBA effects for the sensors that showed significant effects. (F) The individual difference in the size of the GBA in the range of 95–96 Hz recorded from sensor LT44 for the MAE condition as compared to the non-MAE condition shows a significant correlation with the individual difference in the size of the MAE for the two conditions (9 subjects).

source in primary visual cortex and a second, lateral source in parietooccipital cortex close to the location of human area MT+. Only the latter exhibited a significant difference between the MAE and the no-MAE condition, whereas the moment of the V1 dipole did not show a change in its strength between the two conditions. Whereas many studies showed a change in the well known motion induced evoked potentials (motion onset responses), namely an increase in the positive P1 over the occipitotemporal area and a reduction of the negative N200 after motion adaptation (for overview see Mather et al., 1998) there are few electrophysiological studies which actually explore the time during the illusory motion perception. Some groups reported an amplitude increase in the negative N200 component as answer to motion offset after long adaptation (motion presentation) compared to short adaptation (Niedeggen and Wist, 1992) whereas others reported a decrease in the N200 amplitude in the maximally compared to the minimally adapted condition (Hoffmann et al., 1999). Also a positive component has been reported to exclusively change due to adaptation namely to increase in amplitude 160 ms after test stimulus onset (Kobayashi et al., 2002). The only previous electrophysiological investigation offering a more or less exact cortical basis of the MAE in humans has been contributed by Uusitalo and colleagues (1997). In this study, subjects were exposed to a rotating or stationary central stimulus respectively for 1 s, succeeded by a blank period of 2 s duration in which only a fixation spot was visible. In 4 of the 7 subjects, sustained magnetic activity, on average arising 200–500 ms after offset of the adapting stimulus, was significantly smaller if instead of the rotating stimulus a stationary stimulus had been presented. Resorting to a multi-

dipole model the authors could localize a dipole between the occipital and temporal lobe, partly explaining this difference in sustained activity (80–800 ms) in 1 subject (Uusitalo et al., 1997). A major limitation of this study was the lack of a direct measurement of motion perception due to adaptation on a trial to trial basis. Largely qualitative information on the absence or presence of an MAE was based on verbal reports subjects provided after the experiment. A second, quite recent study investigating the velocity aftereffect reported decreased response amplitudes to motion stimuli in the direction of a previously shown adaptation stimulus compared to the response to motion stimuli in the direction opposite to the adapted one. This change in response was observed 200–300 ms after test stimulus onset and was located mainly in the temporooccipital area (Amano et al., 2005).

Our consistent demonstration of a later, parietooccipital dipole specifically related to the occurrence of an MAE, quantitatively demonstrated with state-of-the-art psychophysical techniques supports and extends these earlier observations, suggesting a role of area MT+ in the generation of an MAE. The fact that the latency as well as the localization of the parietooccipital dipole deviated slightly in our second study, in which the visual stimuli had been moved to the other side, is most probably a consequence of the much higher noise level in this experiment compared to experiment 1. These two MEG studies, the one by Uusitalo and the one at hand, suggesting differential roles of early and later parts of visual cortex in the generation of the MAE, are fully compatible with the results obtained by recent TMS and fMRI studies. As described in the Introduction, both approaches have singled out the MT+ complex as connected to the MAE in man. On the other hand,

fMRI failed to reveal specific BOLD responses associated with the occurrence of an MAE in primary visual cortex (Tootell et al., 1995; He et al., 1998; Culham et al., 1999; Taylor et al., 2000; Hautzel et al., 2001).

The second electrophysiological signature of the MAE in this study was oscillatory activity in the gamma-band range. In our study induced gamma-band activity (GBA) reflecting the MAE was observed in channels over two locations. In general a significant change in GBA observed in a single sensor only might at first sight seem implausible since one source evokes a dipole structured magnetic pattern. However single sensors are often observed to be significant (Kaiser et al., 2000, 200; Lutzenberger et al., 2002) and Kaiser and colleagues offer a nice explanation. They argue that a singular GBA can be explained by assuming a more complicated underlying source structure and executing simulations they could show that quadrupoles and even more octopoles or circular currents yield a strong maximum between the sources but considerably weaker minima on the outside. It is very likely that only these maxima reach statistical significance. Importantly this model would also imply that the sources are located close to the area below the sensor with the highest GBA (Kaiser et al., 2000).

The first sensor that showed a relation between GBA and MAE was found over parietooccipital cortex contralateral to the side of the visual field stimulated, a location which is in principle compatible with a source in dorsal extrastriate cortex, although all efforts failed to accurately localize the source. GBA was observed during the period of time in which an incoherent random dot pattern (RDP) was present but perceived as moving due to preceding adaptation. Importantly, the strength of gamma oscillations in the parietooccipital location, most probably reflecting processing in underlying cortex, was not related to the size of the MAE measured in the individual subject.

In order to come up with an interpretation of the emergence of parietooccipital gamma oscillations during the emergence of an MAE, but not quantitatively related to its size, it is pertinent to consider previous observations and thoughts on the possible neuronal basis of the MAE. It has been suggested by Mather et al. (1998) that exposure to a strong motion stimulus not only leads to a decrease in the activity of neurons with a preferred direction matching the direction of the adapting stimulus but also to an increase in the complementary pool of neurons, sharing a preferred direction opposite to the adapted one. This latter increase is thought to be a consequence of reduced inhibition from the former pool of neurons and both changes, the decrease of firing in the adapted pool and the increased firing in the complementary pool, are thought to take part in the formation of the MAE (see Mather and Harris, 1998). The fact that neurons in monkey area MT indeed show a reduced responsiveness after adaptation in the preferred direction, however, an enhancement after adaptation in the null direction, is in full support of this view (Kohn and Movshon, 2003; Petersen et al., 1985). Hence, the formation of an MAE is accompanied by an increase in the firing of a group of neurons sharing a certain preferred direction, similar to the increase in firing resulting from an increase in motion coherence in standard random dot pattern (Britten et al., 1992; Newsome et al., 1989; Britten et al., 1996). Interestingly, in humans GBA has been found to correlate positively with increasing motion coherence in RDPs (Siegel et al., 2006) at a very similar sensor distribution as our parietooccipital gamma focus. Hence, increasing motion coherence enhances the spiking rates of MT neurons and in humans, increasing motion coherence is associated

with increases in GBA. The tentative conclusion to be drawn from these observations then might be that any condition leading to the selective activation of neurons sharing the same trigger feature will lead to increases in spiking activity as well as the formation of GBA, of course suggesting a common mechanistic basis of the two. Actually, synchronous oscillations, most likely underlying the extracortical electromagnetic field oscillations detected by MEG, are known to occur more frequently between neurons sharing the same preferences. For instance, V1 neurons with similar preferred stimulus features show synchronous firing in the gamma range when activated jointly by a preferred stimulus in cat (Eckhorn et al., 1998; Gray and Singer, 1989; Freiwald et al., 1995) and monkey (Ts'o et al., 1986; Livingstone, 1996). In monkeys, it could, moreover, be shown that the neuronal coherence is the higher the more similar the orientation preferences of neurons are (Frien and Eckhorn, 2000). Similar findings have been observed in monkey area MT (Kreiter and Singer, 1996). Actually, the odd one out is motion coherence, whose study has as yet yielded conflicting results as one group found gamma oscillation in area MT to correlate with motion coherence (Nase et al., 2003) whereas another one failed (Bair et al., 2001).

As pointed out in the Introduction section, the emergence of GBA has been interpreted as a possible correlate of increased binding between features leading to a coherent percept. However, in studies of coherent motion perception, it is clear that the emergence of GBA does not coincide with the threshold of the perception of global motion (Siegel et al., 2006). Rather, GBA increases monotonically with the amount of coherence in the stimulus and, actually, there is a stronger increase in GBA between 50% coherence and 100% compared to 12.5% and 25% even though the detection threshold is at about 14%. By the same token, also the parietooccipital GBA in the study at hand, occurring during the perception of an MAE, did not correlate with the strength of the MAE. Hence, at least parietooccipital GBA, while preferring conditions that may lead to specific global percepts, can hardly be their mechanistic basis. Rather, parietooccipital GBA seems to reflect the extent of selective activation of a set of neurons, sharing the same trigger features.

Unlike the parietooccipital GBA, the second, posterior GBA focus did show a correlation with the percept and was increased in subjects exhibiting a higher MAE compared to those showing a lower one. That this GBA was indeed correlated with the MAE and was not related to coarse eye movements is important to note even though we cannot exclude involvement of microsaccades due to the low temporal resolution of our eyetracker (50 Hz). Unfortunately, it was not possible to conclusively locate the point of origin of this activity. Two sources seem conceivable, namely primary visual cortex and the cerebellum. Since dealing with strong visual stimuli the first explanation might seem more intuitive. However, several considerations militate against the interpretation that GBA in this posterior location, correlating with the strength of the perceived MAE, originates from early visual cortex. 1. TMS of human MT+ was reported to disrupt the perception of the MAE, while TMS of V1 did not (Théoret et al., 2002). 2. By the same token, the fMRI studies discussed in detail earlier failed to demonstrate MAE-associated BOLD activations in V1 (Culham et al., 1999; Taylor et al., 2000; Hautzel et al., 2001). 3. The percept-related GBA was not observed contralateral to the hemifield stimulated but ipsilateral to it, obviously at odds with the crossed nature of the visual system.

An area we might expect to exhibit an ipsilateral activation because of its crossed connection with the cerebrum is the

cerebellum. That the detection of activity coming from the cerebellum is by no means impossible for MEG has been shown repeatedly since neuromagnetic activity could be located by means of ECD models (Tesche and Karhu, 2000) as well as by applying beamforming techniques (Timmermann et al., 2003; Gross et al., 2002). If the posterior GBA observed in our experiment indeed originated from the cerebellum, a concern, close at hand would of course be that it reflected the hand movement required by the paradigm rather than the MAE. However, this concern can be dispelled clearly as the topographically circumscribed posterior GBA was found ipsilateral to the moving hand movement in experiment 1 but contralateral to it in experiment 2. The idea of a cerebellar involvement in the MAE is actually less odd as it may appear at first sight as also a recent PET study by Hautzel et al. (2001) has implicated the cerebellum in this perceptual illusion. These authors reported changes in the metabolic signal following motion adaptation not only in MT+ but also within the cerebellar cortex. However, Hautzel and colleagues argue that it was not specifically the MAE which was represented in the cerebellar activity since in a further reference condition with identical attentional demand but no perception of an MAE an elevated cerebellar BOLD signal was found as well.

A role of the cerebellum in the processing of visual motion, possibly suggested by our experiment, would in principle be in accordance with the finding of quite specific deficits of visual motion perception in patients suffering from cerebellar disease (Ivry and Diener, 1991; Nawrot and Rizzo, 1995, 1998; Thier et al., 1999). This prompts the interesting question, if patients suffering from cerebellar disease might also manifest an altered MAE. Obviously, this would have to be expected if the visual motion perception deficit exhibited by patients and an MAE associated cerebellar GBA both reflected a common specific role of the cerebellum in visual motion processing.

## Acknowledgments

## References

Amano, K., Kuriki, I., Takeda, T., 2005. Direction-specific adaptation of magnetic responses to motion onset. Vision Res. 45, 2533–2548.

Bair, W., Zohary, E., Newsome, W.T., 2001. Correlated firing in macaque visual area MT: time scales and relationship to behavior. J. Neurosci. 21 (5), 1676–1697.

Basar-Eroglu, C., Struber, D., Schurmann, M., Stadler, M., Basar, E., 1996. Gamma-band responses in the brain: a short review of psychophysiological correlates and functional significance. Int. J. Psychophysiol. 24, 101–112.

Bertrand, O., Tallon-Baudry, C., 2000. Oscillatory gamma activity in humans: a possible role for object representation. Int. J. Psychophysiol. 38, 211–223.

Blair, R.C., Karniski, W., 1993. An alternative method for significance testing of waveform difference potentials. Psychophysiology 30, 518–524.

Britten, K.H., Shadlen, M.N., Newsome, W.T., Movshon, J.A., 1992. The analysis of visual motion: a comparison of neuronal and psychophysical performance. J. Neurosci. 12, 4745–4765.

Britten, K.H., Newsome, W.T., Shadlen, M.N., Celebrini, S., Movshon, J.A., 1996. A relationship between behavioral choice and the visual responses of neurons in macaque MT. Vis. Neurosci. 13, 87–100.

Clochon, P., Fontbonne, J., Lebrun, N., Etevenon, P., 1996. A new method for quantifying EEG event-related desynchronization: amplitude envelope analysis. Electroencephalogr. Clin. Neurophysiol. 98 (2), 126–129.

Culham, J.C., Dukelow, S.P., Vilis, T., Hassard, F.A., Gati, J.S., Menon, R.S., Goodale, M.A., 1999. Recovery of fMRI activation in motion area MT following storage of the motion aftereffect. J. Neurophysiol. 81 (1), 388–393.

Eckhorn, R., Bauer, R., Jordan, W., Brosch, M., Kruse, W., Munk, M., Reitboeck, H.J., 1998. Coherent oscillations: a mechanism of feature linking in the visual cortex? Multiple electrode and correlation analyses in the cat. Biol. Cybern. 60, 121–130.

Engel, A.K., Singer, W., 2001. Temporal binding and the neural correlates of sensory awareness. Trends Cogn. Sci. 5 (1), 16–25.

Fell, J., Klaver, P., Lehnertz, K., Grunwald, T., Schaller, C., Elger, C.E., Fernandez, G., 2001. Human memory formation is accompanied by rhinal–hippocampal coupling and decoupling. Nat. Neurosci. 4 (12), 1259–1264.

Freiwald, W.A., Kreiter, A.K., Singer, W., 1995. Stimulus dependent intercolumnar synchronization of single unit responses in cat area 17. NeuroReport 6 (17), 2348–2352.

Freunberger, R., Klimesch, W., Sauseng, P., Griesmayr, B., Höller, Y., Pecherstorfer, T., Hanslmayr, S., 2007. Gamma oscillatory activity in a visual discrimination task. Brain Res. Bull. 71, 593–600.

Frien, A., Eckhorn, R., 2000. Functional coupling shows stronger stimulus dependency for fast oscillations than for low-frequency components in striate cortex of awake monkey. Eur. J. Neurosci. 12, 1466–1478.

Fries, P., Reynolds, J.H., Rorie, A.E., Desimone, R., 2001. Modulation of oscillatory neuronal synchronization by selective visual attention. Science 291, 1560–1563.

Fröhlich, F.W., 1913. Beiträge zur allgemeinen Physiologie der Sinnesorgane. Z. Sinnesphysiol. 48, 28–164.

Gray, C.M., 1999. The temporal correlation hypothesis review of visual feature integration: still alive and well. Neuron 24, 31–47.

Gray, C.M., Singer, W., 1989. Stimulus-specific neuronal oscillations in orientation columns of cat visual cortex. Proc. Natl. Aacd. Sci. 86, 1698–1702.

Gross, J., Timmermann, L., Kujala, J., Dirks, M., Schmitz, F., Salmelin, R., Schnitzler, A., 2002. The neural basis of intermittent motor control in humans. Proc. Natl. Aacd. Sci. 99 (4), 2299–2302.

Gruber, T., Müller, M.M., Keil, A., Elbert, T., 1999. Selective visual–spatial attention alters induced gamma band responses in the human EEG. Clin. Neurophysiol. 110, 2074–2085.

Hautzel, H., Taylor, J.G., Krause, B.J., Schmitz, N., Tellmann, L., Ziemons, K., Shah, N.J., Herzog, H., Muller-Gartner, H.W., 2001. The motion aftereffect: more than area V5/MT? Evidence from 15O-butanol PET studies. Brain Res. 892 (2), 281–292.

He, S., Cohen, E.C., Hu, X., 1998. Close correlation between activity in brain area MT/V5 and the perception of a visual motion aftereffect. Curr. Biol. 8, 1215–1218.

Herrmann, C.S., Mecklinger, A., Pfeifer, E., 1999. Gamma responses and ERPs in a visual classification task. Clin. Neurophysiol. 110, 636–642.

Hoffmann, M., Dorn, T.J., Bach, M., 1999. Time course of motion adaptation: motion-onset visual evoked potentials and subjective estimates. Vision Res. 39, 437–444.

Ivry, R.B., Diener, H.C., 1991. Impaired velocity perception in patients with lesions of the cerebellum. J. Cogn. Neurosci. 3, 355–366.

Kahana, K.J., 2006. The cognitive correlates of human brain oscillations. J. Neurosci. 26 (6), 1669–1672.

Kaiser, J., Lutzenberger, W., 2004. Human gamma-band activity: a window to cognitive processing. NeuroReport 16 (3), 207–211.

Kaiser, J., Lutzenberger, W., Preissl, H., Ackermann, H., Birbaumer, N., 2000. Right-hemisphere dominance for the processing of sound-source lateralization. J. Neurosci. 20 (17), 6631–6639.

Kaiser, J., Bühler, M., Lutzenberger, W., 2004. Magnetoencephalographic

gamma-band responses to illusory triangles in humans. NeuroImage 23, 551–560.

Kaiser, J., Hertrich, I., Ackermann, H., Lutzenberger, W., 2006. Gamma-band activity over early sensory areas predicts detection of changes in audiovisual stimuli. NeuroImage 30, 1376–1382.

Keil, A., Müller, M.M., Ray, W.J., Gruber, T., Elbert, T., 1999. Human gamma band activity and perception of a gestalt. J. Neurosci. 19 (16), 7152–7161.

Kobayashi, Y., Yoshino, A., Ogasawara, T., Nomura, S., 2002. Topography of evoked potentials associated with illusory motion perception as a motion aftereffect. Cogn. Brain Res. 13, 75–84.

Kohn, A.J., Movshon, A., 2003. Neuronal adaptation to visual motion in area MT of the macaque. Neuron 39, 681–691.

Krishnan, G.P., Patrick, C.A., Skosnik, D., Vohs, J.L., Busey, T.A., O'Donnell, B.F., 2005. Relationship between steady-state and induced gamma activity to motion. NeuroReport 16 (6), 625–630.

Kreiter, A.K., Singer, W., 1996. Stimulus-dependent synchronization of neuronal responses in the visual cortex of the awake macaque monkey. J. Neurosci. 76 (7), 2381–2396.

Lachaux, J.-P., George, N., Tallon-Baudry, C., Martinerie, J., Hugueville, L., Minotti, L., Kahane, P., Renault, B., 2005. The many faces of the gamma band response to complex visual stimuli. NeuroImage 25, 491–501.

Lakatosa, P., Szilagyib, N., Pinczea, Z., Rajkaia, C., Ulberta, I., Karmosa, G., 2004. Attention and arousal related modulation of spontaneous gamma-activity in the auditory cortex of the cat. Cogn. Brain Res. 19, 1–9.

Lieberman, H.R., Pentland, A.P., 1982. Microcomputer-based estimation of psychophysical thresholds: the best PEST. Behav. Res. Methods Instrum. 14, 21–25.

Livingstone, M.S., 1996. Oscillatory firing and interneuronal correlations in squirrel monkey striate cortex. J. Neurophysiol. 75, 2467–2485.

Lutzenberger, W., Pulvermüller, F., Elbert, T., Birbaumer, N., 1995. Visual stimulation alters local 40-Hz responses in humans: an EEG-study. Neuroscience Letters 183, 39–42.

Lutzenberger, W., Ripper, B., Busse, L., Birbaumer, N., Kaiser, J., 2002. Dynamics of gamma band activity during an audiospatial working memory task in humans. J. Neurosci. 22, 5630–5638.

Mather, G., Harris, J., 1998. Theoretical models of the motion aftereffect. In: Mather, G., Verstraten, F., Anstis, S. (Eds.), The Motion Aftereffect: A Modern Perspective. MIT Press, Cambridge, MA, pp. 157–184.

Mather, G., Verstraten, F., Anstis, S. (Eds.), 1998. The Motion Aftereffect: A Modern Perspective. MIT Press, Cambridge, MA.

McKee, S.P., Klein, S.A., Teller, D.Y., 1985. Statistical properties of forced choice psychometric functions: implications of probit analysis. Percept. Psychophys. 37, 286–298.

Miltner, W.R., Braun, C., Arnold, M., Witte, H., Taub, E., 1999. Coherence of gamma-band EEG activity as a basis for associative learning. Nature 397, 434–436.

Müller, M.M., Bosch, J., Elbert, T., Kreiter, A., Valdes Sosa, M., Valdes Sosa, P., Rockstroh, B., 1996. Visually induced gamma-band responses in human electroencephalographic activity—a link to animal studies. Exp. Brain Res. 112, 96–102.

Müller, M.M., Gruber, T., Keil, A., 2000. Modulation of induced gamma band activity in the human EEG by attention and visual information processing. Int. J. Psychophysiol. 38, 283–299.

Nase, G., Singer, W., Monyer, H., Engel, A.K., 2003. Features of neuronal synchrony in mouse visual cortex. J. Neurophysiol. 90, 1115–1123.

Nawrot, M., Rizzo, M., 1995. Motion perception deficit from midline cerebellar lesions in human. Vis. Res. 3, 723–731.

Nawrot, M., Rizzo, M., 1998. Chronic motion perception deficits from midline cerebellar lesions in human. Vision Res. 38, 2219–2224.

Newsome, T.W., Kenneth, H., Britten, K.H., Movshon, J.A., 1989. Neuronal correlates of a perceptual decision. Nature 341, 52–54.

Niedeggen, M., Wist, E.R., 1992. Detection of motion direction is correlated with motion-evoked potentials. Perception 23, 32.

Noreen, E.W., 1989. Computer Intensive Methods for Testing Hypotheses: An introduction. Wiley, New York.

Petersen, S.E., Baker, J.F., Allman, J.M., 1985. Direction-specific adaptation in area MT of the owl monkey. Brain Res. 346, 146–150.

Purkinje, J.E., 1825. Beobachtungen und Versuche zur Physiologie der Sinne. Neue Beitrage zur Kenntniss des Sehens in subjektiver Hinsicht. Reimer, Berlin.

Robinson, S.E., Vrba, J., 1999. Functional neuroimaging by synthetic aperture magnetometry (SAM). Recent Advances in Biomagnetism. Tohoku Univ. Press, Sendai, pp. 302–305.

Rodriguez, E., George, N., Lachaux, J.P., Martinerie, J., Renault, B., Varela, F.J., 1999. Perception's shadow: long-distance synchronization of human brain activity. Nature 397, 430–433.

Rose, M., Büchel, C., 2005. Neural coupling binds visual tokens to moving stimuli. J. Neurosci. 25 (44), 10101–10104.

Siegel, M., Donner, T., Oostenveld, R., Fries, P., Engel, A., 2006. High-frequency activity in human visual cortex is modulated by visual motion strength. Cereb. Cortex 17, 732–741.

Singer, W., 1999. Neuronal synchrony: a versatile code for the definition of relations? Neuron 24, 49–65.

Sokolov, A., Lutzenberger, W., Pavlova, M., Preissl, H., Braun, C., Birbaumer, N., 1999. Gamma-band MEG activity to coherent motion depends on task-driven attention. Neuroreport 10, 1997–2000.

Tallon-Baudry, C., 2003. Oscillatory synchrony and human visual cognition. J. Physiol. (Paris) 97, 355–363.

Tallon-Baudry, C., Bertrand, O., Delpuech, C., Pernier, J., 1996. Stimulus specificity of phase-locked and non-phase-locked 40 Hz visual responses in humans. J. Neurosci. 16, 4240–4249.

Tallon-Baudry, C., Bertrand, O., Delpuech, C., Pernier, J., 1997. Oscillatory gamma-band (30–70 Hz) activity induced by a visual search task in humans. J. Neurosci. 17 (2), 722–734.

Tallon-Baudry, C., Bertrand, O., Peronnet, F., Pernier, J., 1998. Induced g-band activity during the delay of a visual short-term memory task in humans. J. Neurosci. 18 (11), 4244–4254.

Tallon-Baudry, C., Bertrand, O., Henaff, M.A., Isnard, J., Fischer, C., 2005. Attention modulates gamma-band oscillations differently in the human lateral occipital cortex and fusiform gyrus. Cereb. Cortex 15, 654–662.

Taylor, M.M., Creelman, C.D., 1967. PEST: efficient estimates on probability functions. J. Acoust. Soc. Am. 41, 782–787.

Taylor, J.G., Schmitz, N., Ziemons, K., Grosse-Ruyken, M.L., Gruber, O., Mueller-Gartner, H.W., Shah, N.J., 2000. The network of brain areas involved in the motion aftereffect. NeuroImage 11, 257–270.

Tesche, C.D., Karhu, J., 2000. Anticipatory cerebellar responses during somatosensory omission in man. Hum. Brain Mapp. 9, 119–142.

Théoret, H., Kobayashi, M., Ganis, G., Di Capua, P., Pascual-Leone, A., 2002. Repetitive transcranial magnetic stimulation of human area MT/V5 disrupts perception and storage of the motion aftereffect. Neuropsychologia 40, 2280–2287.

Thier, P., Haarmeier, T., Treue, S., Barash, S., 1999. Absence of a common functional denominator of visual disturbances in cerebellar disease. Brain 122, 2133–2146.

Timmermann, L., Gross, J., Dirks, M., Volkmann, J., Freunds, H.J., Schnitzler, A., 2003. The cerebral oscillatory network of parkinsonian resting tremor. Brain 126, 199–212.

Tootell, R.B.H., Reppas, J.B., Dale, A.M., Look, R.B., Sereno, M.I., Malach, R., Brady, T.J., Rosen, B.R., 1995. Visual motion aftereffect in human cortical area MT+ revealed by functional magnetic resonance imaging. Nature 375, 139–141.

Trautner, P., Rosburg, T., Dietl, T., Fell, J., Korzyukov, O.A., Kurthen, M., Schaller, C., Elger, C.E., Boutros, N.N., 2006. Sensory gating of auditory evoked and induced gamma band activity in intracranial recordings. NeuroImage 32, 790–798.

Ts'o, D.Y., Gilbert, C.D., Wiesel, T.N., 1986. Relationships between horizontal interactions and functional architecture in cat striate cortex as revealed by cross-correlation analysis. J. Neurosci. 6, 1160–1170.

Uusitalo, M.A., Virsu, V., Salenius, S., Nasanen, R., Hari, R., 1997. Activation of human V5 complex and rolandic regions in association with moving visual stimuli. NeuroImage 5, 241–250.

Wohlgemuth, A., 1911. On the aftereffect of seen movement. Br. J. Psychol., Monogr. Suppl. 1, 1–117.